

Holographic dark energy in a Universe with spatial curvature and massive neutrinos: a full Markov Chain Monte Carlo exploration

Shuang Wang,^{1,2} Yun-He Li,¹ Xiao-Dong Li,^{3,4} and Xin Zhang^{*1,5,†}

¹*Department of Physics, College of Sciences,*

Northeastern University, Shenyang 110004, China

²*Homer L. Dodge Department of Physics & Astronomy,*

Univ. of Oklahoma, 440 W Brooks St., Norman, OK 73019, U.S.A.

³*Institute of Theoretical Physics, Chinese Academy of Sciences, Beijing 100190, China*

⁴*Kavli Institute for Theoretical Physics China,*

Chinese Academy of Sciences, Beijing 100190, China

⁵*Center for High Energy Physics, Peking University, Beijing 100080, China*

Abstract

In this paper, we report the results of constraining the holographic dark energy model with spatial curvature and massive neutrinos, based on a Markov Chain Monte Carlo global fit technique. The cosmic observational data include the full WMAP 7-yr temperature and polarization data, the type Ia supernova data from Union2.1 sample, the baryon acoustic oscillation data from SDSS DR7 and WiggleZ Dark Energy Survey, and the latest measurements of H_0 from HST. To deal with the perturbations of dark energy, we adopt the parameterized post-Friedmann method. We find that, for the simplest holographic dark energy model without spatial curvature and massive neutrinos, the phenomenological parameter $c < 1$ at more than 4σ confidence level. The inclusion of spatial curvature enlarges the error bars and leads to $c < 1$ only in about 2.5σ range; in contrast, the inclusion of massive neutrinos does not have significant influence on c . We also find that, for the holographic dark energy model with spatial curvature but without massive neutrinos, the 3σ error bars of the current fractional curvature density Ω_{k0} are still in order of 10^{-2} ; for the model with massive neutrinos but without spatial curvature, the 2σ upper bound of the total mass of neutrinos is $\sum m_\nu < 0.48$ eV. Moreover, there exists clear degeneracy between spatial curvature and massive neutrinos in the holographic dark energy model, which enlarges the upper bound of $\sum m_\nu$ by more than 2 times. In addition, we demonstrate that, making use of the full WMAP data can give better constraints on the holographic dark energy model, compared with the case using the WMAP “distance priors”.

PACS numbers: 98.80.-k, 95.36.+x.

^{*} Corresponding author

[†]Electronic address: zhangxin@mail.neu.edu.cn

I. INTRODUCTION

Observations of type Ia supernovae (SNIa) [1], cosmic microwave background (CMB) [2] and large scale structure (LSS) [3] all indicate that the Universe is undergoing an accelerating expansion. This implies the existence of a mysterious component, called dark energy [4], which has negative pressure and takes the largest proportion of the total density in the present Universe. In the past fifteen years, lots of efforts [5–13] have been made to understand dark energy, yet we still know little about its nature.

In this paper we focus on the holographic dark energy model, which is a quantum gravity approach to the dark energy problem [14]. In this model, the vacuum energy is viewed as dark energy, and is related to the event horizon of the Universe when we require that the zero-point energy of the system should not exceed the mass of a black hole with the same size [15]. In this way, we have the holographic dark energy density [16]

$$\rho_{de} = 3c^2 M_{Pl}^2 R_h^{-2}, \quad (1)$$

where c is a dimensionless phenomenological parameter which plays an important role in determining the properties of the holographic dark energy, M_{Pl} is the reduced Planck mass, and R_h is the future event horizon size of the Universe, defined as

$$R_h = a \int_t^\infty \frac{dt}{a} = a \int_a^\infty \frac{da}{Ha^2}. \quad (2)$$

The holographic dark energy model has been proven to be a competitive and promising dark energy candidate. It can theoretically explain the coincidence problem [16], and is proven to be perturbational stable [17]. Moreover, it is favored by the observational data [18]. For more studies on the holographic dark energy model, see, e.g., [19–23].

It is fairly difficult to calculate the cosmological perturbations of dark energy in the holographic dark energy model, because there is a non-local effect making the calculation of perturbations extremely hard to be treated. Thus, in the past, for the CMB observations, only the WMAP “distance priors” data were used to constrain the holographic dark energy model in order to avoid the inclusion of the perturbations of dark energy (see e.g. Refs. [24–28]). However, recently, it has been realized that, in order to make progress one should first ignore the non-local effect in the holographic dark energy model and directly calculate the perturbations of holographic dark energy as if it is a usual dynamical dark energy. Along this line, in a recent work [29], a global fitting analysis on the holographic dark energy model was performed. By using the 557 SNIa data from Union2 sample [30], the baryon acoustic oscillation (BAO) data from SDSS DR7 [31], and the full CMB information from WMAP 7-yr observations [32], the author obtained

$c = 0.696^{+0.0736+0.159+0.264}_{-0.0737-0.132-0.190}$ at $1, 2, 3\sigma$ confidence levels (CL), showing that the future Universe will be dominated by phantom dark energy at 3σ CL. However, in Ref. [29] it is not mentioned how the divergence problem concerning the $w = -1$ -crossing is treated.

In this paper, we shall perform a global fit analysis on the holographic dark energy model with spatial curvature and massive neutrinos. As argued in Ref. [33], the numerical studies of dynamical dark energy should include the current fractional curvature density Ω_{k0} as a free parameter to be fitted alongside the equation-of-state (EOS) parameters w of dark energy. In addition, the total mass of neutrinos $\sum m_\nu$ is also tightly correlated with w [34]. So, in our work, based on a Markov Chain Monte Carlo (MCMC) global fit technique, we will consider spatial curvature and massive neutrinos in the holographic dark energy model, and will deeply analyze the influences of these two factors on the fitting results. In a dynamical dark energy model, one must be careful about the treatment of perturbations in dark energy when w crosses -1 . In this work we use the “parameterized post-Friedmann” (PPF) approach [35] implemented in the CAMB code following the WMAP team.

This paper is organized as follows. In Section II, we derive the basic equations for the holographic dark energy in a Universe with spatial curvature and massive neutrinos. In Section III, we introduce the methodology and the observational data, and then give the data-fitting results. At last, some concluding remarks are given in Section IV. In this work, we assume today’s scale factor $a_0 = 1$, so the redshift z satisfies $z = a^{-1} - 1$; the subscript “0” always indicates the present value of the corresponding quantity, and the unit with $c = \hbar = 1$ is used.

II. HOLOGRAPHIC DARK ENERGY MODEL WITH SPATIAL CURVATURE AND MASSIVE NEUTRINOS

In this section, we derive the basic equations for the holographic dark energy model with spatial curvature and massive neutrinos.

A. Friedmann equations in a non-flat Universe

In a spatially non-flat Friedmann-Robertson-Walker Universe, the Friedmann equation can be written as

$$3M_{Pl}^2 H^2 = \rho_k + \rho_{dm} + \rho_{de} + \rho_b + \rho_\nu + \rho_r, \quad (3)$$

where $\rho_k = -3M_{Pl}^2 \frac{k}{a^2}$ is the effective energy density of the curvature component, ρ_{dm} , ρ_{de} , ρ_b , ρ_ν and ρ_r represent the energy density of dark matter, dark energy, baryon, massive neutrinos and radiation, respectively. Notice that we adopt the approximate method used in the five-year analysis of WMAP [36]: dividing

neutrino component into the relativistic neutrinos and the massive neutrinos, and including the relativistic neutrinos into radiation component. For convenience, we define the fractional energy densities of the various components,

$$\Omega_k = \frac{-k}{H^2 a^2} = \frac{\rho_k}{\rho_c}, \quad \Omega_{dm} = \frac{\rho_{dm}}{\rho_c}, \quad \Omega_{de} = \frac{\rho_{de}}{\rho_c}, \quad \Omega_b = \frac{\rho_b}{\rho_c}, \quad \Omega_\nu = \frac{\rho_\nu}{\rho_c}, \quad \Omega_r = \frac{\rho_r}{\rho_c}, \quad (4)$$

where $\rho_c = 3M_{pl}^2 H^2$ is the critical density of the Universe. It is clear that

$$\Omega_k + \Omega_{dm} + \Omega_{de} + \Omega_b + \Omega_\nu + \Omega_r = 1. \quad (5)$$

In addition, the energy conservation equations for the various components take the forms

$$\dot{\rho}_{dm} + 3H\rho_{dm} = 0, \quad (6)$$

$$\dot{\rho}_{de} + 3H(\rho_{de} + p_{de}) = 0, \quad (7)$$

$$\dot{\rho}_b + 3H\rho_b = 0, \quad (8)$$

$$\dot{\rho}_\nu + 3H\rho_\nu = 0, \quad (9)$$

$$\dot{\rho}_r + 4H\rho_r = 0, \quad (10)$$

$$\dot{\rho}_k + 2H\rho_k = 0. \quad (11)$$

Combining Eqs. (6)–(11) together, we can obtain the form of p_{de} ,

$$p_{de} = -\frac{2}{3}\frac{\dot{H}}{H^2}\rho_c - \rho_c - \frac{1}{3}\rho_r + \frac{1}{3}\rho_k. \quad (12)$$

Substituting p_{de} into Eq. (7), we have

$$\left(2\frac{\dot{H}}{H} + \frac{\dot{\Omega}_{de}}{\Omega_{de}} + 3H\right)\rho_{de} + H(\rho_k - \rho_r) - \left(2\frac{\dot{H}}{H} + 3H\right)\rho_c = 0. \quad (13)$$

Dividing the above equation by ρ_c , we get a derivative equation of \dot{H} and $\dot{\Omega}_{de}$,

$$2(\Omega_{de} - 1)\frac{\dot{H}}{H} + \dot{\Omega}_{de} + H(3\Omega_{de} - 3 + \Omega_k - \Omega_r) = 0. \quad (14)$$

B. Holographic dark energy in a non-flat Universe

From the energy density of the holographic dark energy, we have

$$L = \frac{c}{H \sqrt{\Omega_{de}}}. \quad (15)$$

In a non-flat Universe, the IR cut-off length scale L takes the form

$$L = ar(t), \quad (16)$$

and $r(t)$ satisfies

$$\int_0^{r(t)} \frac{dr}{\sqrt{1 - kr^2}} = \int_t^{+\infty} \frac{dt}{a(t)}. \quad (17)$$

By carrying out the integration, we have

$$r(t) = \frac{1}{\sqrt{k}} \sin \left(\sqrt{k} \int_t^{+\infty} \frac{dt}{a} \right) = \frac{1}{\sqrt{k}} \sin \left(\sqrt{k} \int_{a(t)}^{+\infty} \frac{da}{Ha^2} \right). \quad (18)$$

Equation (16) leads to another equation about $r(t)$, namely,

$$r(t) = \frac{L}{a} = \frac{c}{\sqrt{\Omega_{de}} Ha}. \quad (19)$$

Combining Eqs. (18) and (19) yields

$$\sqrt{k} \int_t^{+\infty} \frac{dt}{a} = \arcsin \frac{c \sqrt{k}}{\sqrt{\Omega_{de}} a H}. \quad (20)$$

Taking derivative of Eq. (20) with respect to t , one can get

$$\frac{\dot{\Omega}_{de}}{2\Omega_{de}} + H + \frac{\dot{H}}{H} = \sqrt{\frac{\Omega_{de} H^2}{c^2} - \frac{k}{a^2}}. \quad (21)$$

C. Evolution equations of $E(z)$ and $\Omega_{de}(z)$

Combining Eq. (14) with Eq. (21), we eventually obtain the following two equations governing the dynamical evolution of the holographic dark energy in a Universe with spatial curvature and massive neutrinos,

$$\frac{1}{E(z)} \frac{dE(z)}{dz} = -\frac{\Omega_{de}}{1+z} \left(\frac{\Omega_k - \Omega_r - 3}{2\Omega_{de}} + \frac{1}{2} + \sqrt{\frac{\Omega_{de}}{c^2} + \Omega_k} \right), \quad (22)$$

$$\frac{d\Omega_{de}}{dz} = -\frac{2\Omega_{de}(1 - \Omega_{de})}{1+z} \left(\sqrt{\frac{\Omega_{de}}{c^2} + \Omega_k} + \frac{1}{2} - \frac{\Omega_k - \Omega_r}{2(1 - \Omega_{de})} \right), \quad (23)$$

where $E(z) \equiv H(z)/H_0$ is the dimensionless Hubble expansion rate, and

$$\Omega_k(z) = \frac{\Omega_{k0}(1+z)^2}{E(z)^2}, \quad \Omega_r(z) = \frac{\Omega_{r0}(1+z)^4}{E(z)^2}. \quad (24)$$

The initial conditions are $E(0) = 1$ and $\Omega_{de}(0) = 1 - \Omega_{k0} - \Omega_{dm0} - \Omega_{b0} - \Omega_{\nu0} - \Omega_{r0}$. Note also that $\Omega_{\nu0}$ can be expressed as [32]

$$\Omega_{\nu0} = \frac{\sum m_\nu}{94h^2\text{eV}}, \quad (25)$$

where h is the reduced Hubble constant, and $\sum m_\nu$ is the sum of neutrino masses. In addition, the value of Ω_{r0} is determined by the WMAP 7-yr observations [32]

$$\Omega_{r0} = 2.469 \times 10^{-5} h^{-2} (1 + 0.2271 N_{eff}), \quad (26)$$

where $N_{eff} = 3.04$ is the effective number of neutrino species. Thus, Eqs. (22) and (23) can be solved numerically, and will be used in the data analysis procedure.

In this paper, we shall consider the following four cases: (a) the model of holographic dark energy without spatial curvature and massive neutrinos ($\Omega_{k0} = 0$ and $\sum m_\nu = 0$), denoted as HDE; (b) the model of holographic dark energy with spatial curvature but without massive neutrinos ($\Omega_{k0} \neq 0$ but $\sum m_\nu = 0$), denoted as KHDE; (c) the model of holographic dark energy with massive neutrinos but without spatial curvature ($\sum m_\nu \neq 0$ but $\Omega_{k0} = 0$), denoted as VHDE; (d) the model of holographic dark energy with spatial curvature and massive neutrinos, ($\Omega_{k0} \neq 0$ and $\sum m_\nu \neq 0$), denoted as KVHDE.

III. METHODOLOGY, DATA, AND RESULTS

We have modified the MCMC package ‘‘CosmoMC’’ [37] to perform a global fitting analysis for the considered models. As is known, within the dynamical dark energy models, the perturbations of dark energy are important [38–40] for the global fitting analysis. In this work we calculate the dark energy perturbations by using the formalism of Ma and Bertschinger [41]. Also, we are very careful about the treatment of the divergence problem [42] for the dark energy perturbations when w crosses -1 . We deal with this issue by using the PPF code [35]. This code supports a time-dependent EOS w that is allowed to cross -1 multiple times [43] for the dark energy perturbations. Moreover, it has been widely used in the literature to deal with the perturbations of dark energy (see e.g. Ref. [44]).

Our most general parameter space vector is:

$$\mathbf{P} \equiv (\omega_b, \omega_{dm}, \Theta, \tau, c, \Omega_{k0}, \sum m_\nu, n_s, A_s), \quad (27)$$

where $\omega_b \equiv \Omega_{b0}h^2$ and $\omega_{dm} \equiv \Omega_{dm0}h^2$, Θ is the ratio (multiplied by 100) of the sound horizon to the angular diameter distance at decoupling, τ is the optical depth to re-ionization, c is the phenomenological parameter of the holographic dark energy model, A_s and n_s are the amplitude and the spectral index of the primordial scalar perturbation power spectrum. For the pivot scale, we set $k_{s0} = 0.002\text{Mpc}^{-1}$ to be consistent with the WMAP team [32].

In the computation of the CMB anisotropy, we include the WMAP 7-yr temperature and polarization power spectra [32] with the routine for computing the likelihood supplied by the WMAP team [45]. For the SNIa, we make use of the recently released 580 SNIa data from the “Union2.1” sample [46], where the systematic errors of SNIa are included in our analysis. For the LSS information, we use the BAO data from the SDSS DR7 [31] and WiggleZ Dark Energy Survey [47]. In addition, we also use the latest Hubble space telescope (HST) measurement of the Hubble constant, $H_0 = 73.8 \pm 2.4 \text{ km s}^{-1} \text{ Mpc}^{-1}$ [48].

Before constraining the model parameter space, we study the effects of the phenomenological parameter c on the CMB C_l^{TT} power spectrum by setting different c and fixing the other model parameters. As an example, here we just consider the simplest HDE model. The results are shown in Fig. 1. For comparison, we also plot the results of the XCDM models with different constant w . One can see that, for the HDE models with different c , the main difference appears at low ($l < 20$) multipole momentum parts which correspond to large scales. This means that the main contribution to CMB power spectra from the HDE comes from the evolution of EOS and its domination at the late epoch through late ISW effect. As seen in this figure, a smaller c will yield a smaller C_l^{TT} at low l . Besides, since the EOS of HDE satisfies $w = -\frac{1}{3} - \frac{2\sqrt{\Omega_{de}}}{3c}$ [16], a smaller c will give a smaller w . So for the HDE model, a smaller w will lead to a smaller C_l^{TT} at low l . Similarly, for the XCDM model, a smaller w will also lead to a smaller C_l^{TT} at low l . Thus, the results of the HDE and the XCDM model are consistent with each other.

In the following, we will present the data-fitting results. Table I summarizes the fitting results, including the best-fit and 1, 2, 3 σ values of c and Ω_{k0} , as well as the 2 σ upper bounds of $\sum m_\nu$, for the considered models. Moreover, we list the maximal confidence levels for $c < 1$, in this table. In addition, in Figs. 2–5, we plot the 1D marginalized distributions of individual parameters, as well as the 2D marginalized 1, 2, 3 σ CL contours, for these models. Let us discuss them in detail in what follows.

The fitting results of the HDE model are shown in Fig. 2. We find that the values of c in 1, 2, 3 σ regions are $c = 0.680^{+0.064+0.135+0.222}_{-0.066-0.119-0.159}$; note that the error bars are slightly smaller than those obtained by using the WMAP “distance priors” [28]. Moreover, we find that $c < 1$ at 4.2 σ CL, which means that the future Universe will be dominated by phantom dark energy and will end up with a “big rip” (cosmic doomsday) at more than 4 σ CL. In Ref. [23] it has been demonstrated that $c < 1$ may lead to the ruin of the theoretical foundation—the effective quantum field theory—of the holographic dark energy scenario. To rescue the

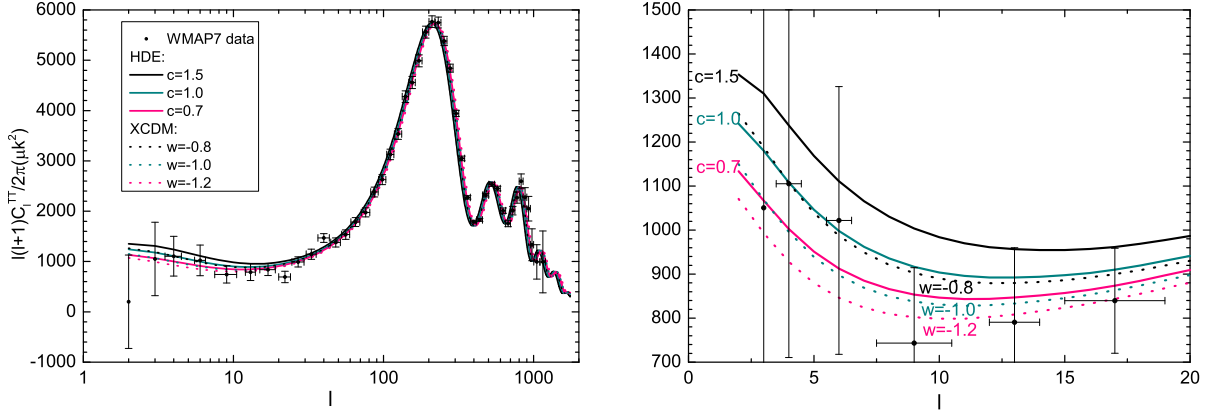


FIG. 1: The effects of the phenomenological parameter c on the CMB C_l^{TT} power spectrum. The black dots with error bars denote the observed data with their corresponding uncertainties from WMAP 7-yr results. The solid lines denote the holographic dark energy models with different c , and the dotted lines denote the XCDM models with different w . For the other model parameters, we adopt their best-fit values given by the WMAP 7-yr observations [32].

TABLE I: Fitting results of the holographic dark energy models

Model	c	Maximal CL for $c < 1$	Ω_{k0}	$\sum m_\nu (2\sigma)$
HDE	$0.680^{+0.064+0.135+0.222}_{-0.066-0.119-0.159}$	4.2σ	—	—
KHDE	$0.702^{+0.104+0.232+0.393}_{-0.063-0.102-0.176}$	2.5σ	$0.004^{+0.009+0.016+0.023}_{-0.004-0.010-0.015}$	—
VHDE	$0.708^{+0.014+0.111+0.159}_{-0.099-0.153-0.215}$	4.6σ	—	$\sum m_\nu < 0.48 \text{ eV}$
KVHDE	$0.733^{+0.037+0.185+0.321}_{-0.107-0.170-0.230}$	2.7σ	$0.010^{+0.010+0.020+0.032}_{-0.004-0.014-0.018}$	$\sum m_\nu < 1.17 \text{ eV}$

holographic scenario of dark energy, one may employ the braneworld cosmology and incorporate the extra-dimension effects into the holographic theory of dark energy. It has been found [23] that such a mend could erase the big-rip singularity and leads to a de Sitter finale for the holographic cosmos. In addition, if there is some direct, non-gravitational interaction between holographic dark energy and dark matter, and such an interaction satisfies some conditions, the big rip can also be avoided [28, 49].

Figure 3 shows the results of the KHDE model. It is seen that, compared with the HDE model, the KHDE model slightly favors a larger best-fit value of c . Moreover, the error bars of c are also enlarged. As shown in Fig. 2, for the HDE model, we have $c < 1$ at more than 4σ CL. However, As shown in Fig. 3, after considering spatial curvature, we have $c < 1$ only in 2.5σ range.

This figure also shows the degeneracy situation of Ω_{k0} and c , in the KHDE model. It is clear that Ω_{k0} and c are in positive correlation. This result is well consistent with our pervious work (see Fig. 4 of [49]; notice that the convention of Ω_{k0} in this paper is different from that in [49]). The best-fit value for Ω_{k0}

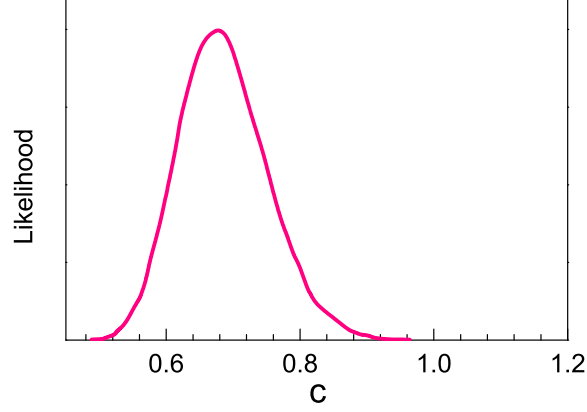


FIG. 2: The 1D marginalized distribution of the phenomenological parameter c , for the HDE model.

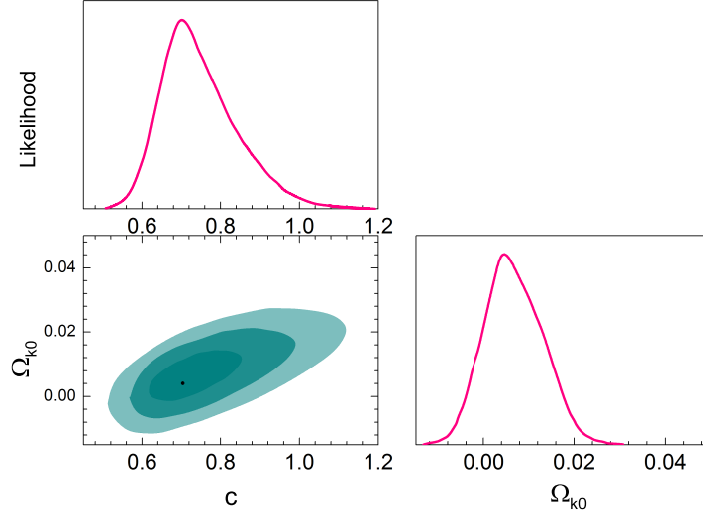


FIG. 3: The 1D marginalized distributions of individual parameters and 2D marginalized 1, 2, 3 σ CL contours, for the KHDE model.

is very close to zero, i.e., $\Omega_{k0} = 0.004$. The 2σ range of the spatial curvature is $-0.006 < \Omega_{k0} < 0.020$. Actually, the 3σ error bars of Ω_{k0} are still fairly small, also in order of 10^{-2} .

The constraints on the VHDE model are shown in Fig. 4. One can see that, compared with the HDE model, the VHDE model also slightly favors a larger best-fit value of c . However, for the VHDE model, the changes on the error bars of c are quite different from the KHDE model: in the KHDE model, both the upper and the lower bounds of c are enlarged comparing to the HDE model; while in the VHDE model, although the lower bounds of c are enlarged, the upper bounds of c are reduced comparing to the HDE model. Moreover, for the VHDE model, we have $c < 1$ at 4.6σ CL, which is quite similar to the result of the simplest HDE model. Therefore, we can conclude that the inclusion of massive neutrinos does not have

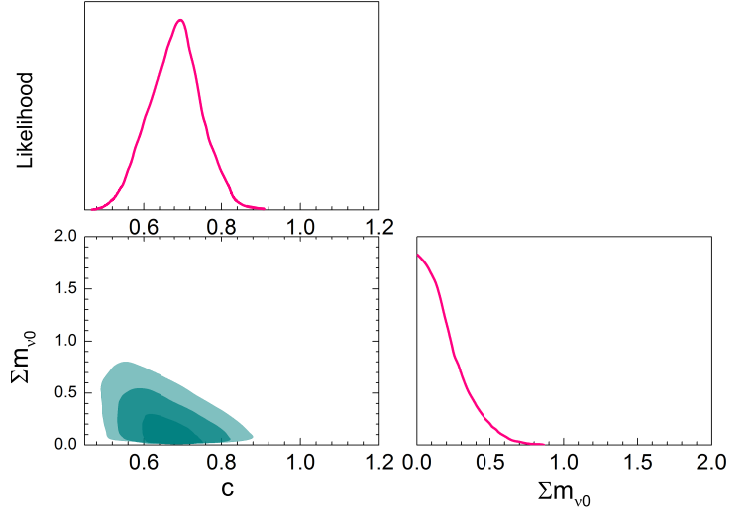


FIG. 4: The 1D marginalized distributions of individual parameters and 2D marginalized 1, 2, 3 σ CL contours, for the VHDE model.

significant influence on the phenomenological parameter c .

From Fig. 4, one can also see that there is no significant correlation between $\sum m_\nu$ and c , in the VHDE model. In addition, we obtain the upper bound of the total mass of neutrinos in the holographic dark energy model, $\sum m_\nu < 0.48$ eV at 2σ CL. This is the first result of the neutrino mass in the holographic dark energy model. For comparison, we mention here some results of neutrino mass in other dark energy scenarios. For a flat Λ CDM model, i.e., $w = -1$ and $\Omega_{k0} = 0$, Komatsu et al. [32] found that the WMAP+BAO+ H_0 limit is $\sum m_\nu < 0.58$ eV (95% CL). For a constant w model the results given by Komatsu et al. [32] are: $\sum m_\nu < 0.71$ eV (95% CL) from WMAP+LRG+ H_0 , and $\sum m_\nu < 0.91$ eV (95% CL) from WMAP+BAO+SN (where SN is the Constitution sample).

The results for the most sophisticated case, i.e. the KVHDE model, are shown in Fig. 5. We find that, for the KVHDE model, we have $c < 1$ only at the 2.7σ level.

This figure also shows the degeneracy situations of various parameters, in the KVHDE models. In the KHDE model we find that Ω_{k0} and c are in positive correlation, and in the VHDE model we do not observe significant correlation between $\sum m_\nu$ and c . So, we believe that the parameters Ω_{k0} and $\sum m_\nu$ should be in positive correlation. Indeed, in the KVHDE model, we find that the result is in accordance with the expectation. In addition, when simultaneously considering spatial curvature and massive neutrinos in the holographic dark energy model, the parameter space of $(\Omega_{k0}, \sum m_\nu)$ is greatly amplified. For example, the upper bound of $\sum m_\nu$ is enlarged by more than 2 times comparing to the VHDE model.

Next, let us discuss the cosmological consequences of introducing spatial curvature and massive neutri-

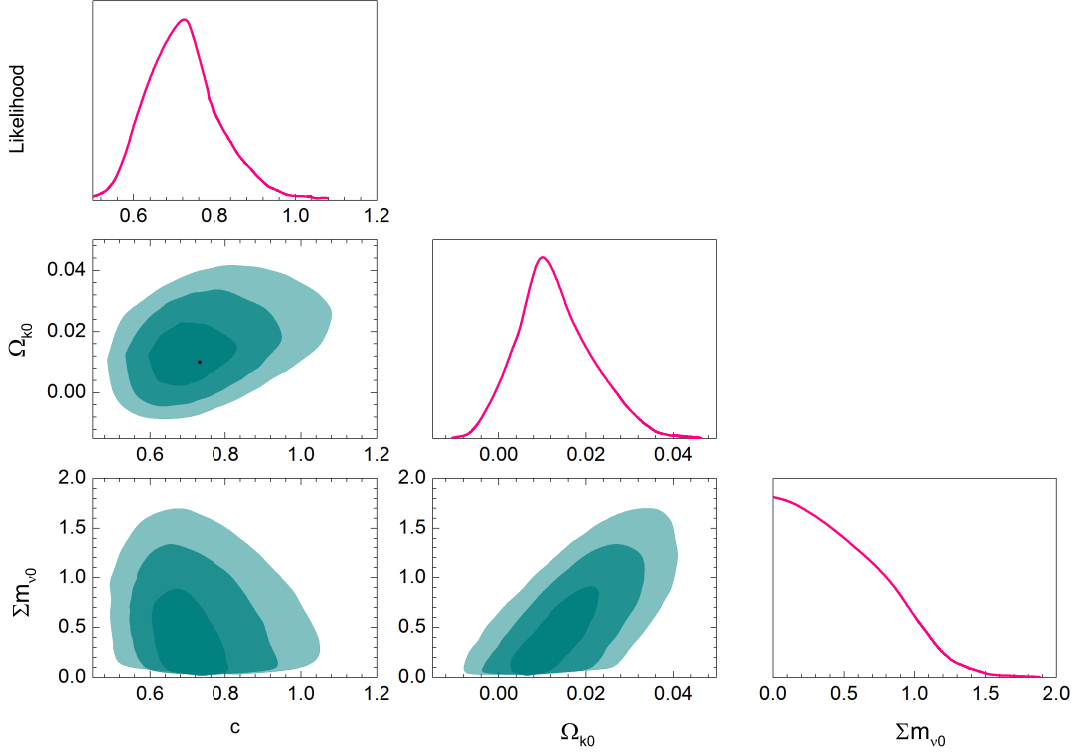


FIG. 5: The 1D marginalized distributions of individual parameters and 2D marginalized 1, 2, 3 σ CL contours, for the KVHDE model.

nos in the holographic dark energy model. In Fig. 6, we plot the CMB C_l^{TT} power spectrum for the HDE, KHDE, VHDE and KVHDE models with the corresponding best-fit parameters. To make a comparison, we also include the Λ CDM model with the best-fit parameters given by the same set of data. Two significant features can be seen in this figure: first, the C_l^{TT} power spectrum for the HDE is well inside the error bars of the observational data given by the WMAP 7-yr measurements and matches to the Λ CDM model very well, this implies that the HDE is a competitive model of dark energy; second, the C_l^{TT} power spectrum for the KHDE, VHDE and KVHDE models almost overlap with the results of the HDE model, showing that the inclusion of spatial curvature and massive neutrinos in the holographic dark energy model does not significantly change the best-fit results.

In Fig. 7, we plot the evolution of $w(z)$ along with redshift z , including the best-fit results, as well as the 1, 2, 3, 4 σ regions, for the considered models. As seen in the left panels of Fig. 7, for the holographic dark energy models without spatial curvature, w will cross -1 at more than 4 σ CL. As mentioned above, this means that the future Universe will be dominated by phantom dark energy and will end up with a “big rip” singularity at more than 4 σ CL. As seen in the right panels of Fig. 7, after introducing the spatial curvature, w will cross -1 only in about 2.5 σ range. Therefore, the inclusion of spatial curvature

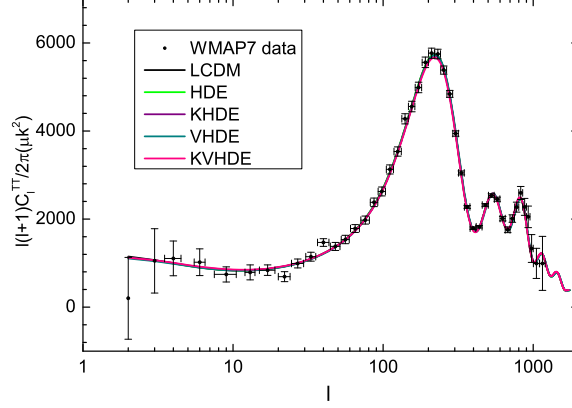


FIG. 6: The CMB C_l^{TT} power spectrum for the HDE, KHDE, VHDE and KVHDE models with the corresponding best-fit parameter values. The black dots with error bars denote the observed data with their corresponding uncertainties from WMAP 7-yr results.

in the holographic dark energy model may be helpful to alleviate the future cosmic doomsday problem. In contrast, the inclusion of massive neutrinos does not have significant influence on the evolution of $w(z)$.

We are also interested in the differences between the cosmological constraints given by the WMAP 7-yr “distance priors” and those given by the full WMAP 7-yr data. As an example, we plot the marginalized $1, 2, 3\sigma$ CL contours in the $c-\Omega_{k0}$ plane, for the KHDE model, in Fig. 8. The pink contours are plotted by using the WMAP “distance priors”, and the olive contours are plotted by using the full WMAP data. As seen in this figure, the regions of the $1, 2, 3\sigma$ contours given by the full WMAP data are significantly smaller than the corresponding regions given by the WMAP “distance priors”. Therefore, making use of the full WMAP data can give better constraints on the holographic dark energy model, compared with the case using the WMAP “distance priors”.

IV. CONCLUDING REMARKS

In this paper we consider the holographic dark energy model with spatial curvature and massive neutrinos. It is well known that both the spatial curvature and neutrino mass are correlated with the dark energy EOS, so it is important to study the influences of these factors to the holographic dark energy. In addition, it is also rather significant to consider the cosmological perturbations in holographic dark energy and make a global fit analysis on the holographic dark energy model.

We placed constraints on the holographic dark energy in a Universe with spatial curvature and massive neutrinos, based on a MCMC global fit technique. The cosmic observational data include the WMAP 7-yr temperature and polarization data, the SNIa data from Union2.1 sample, the BAO data from SDSS

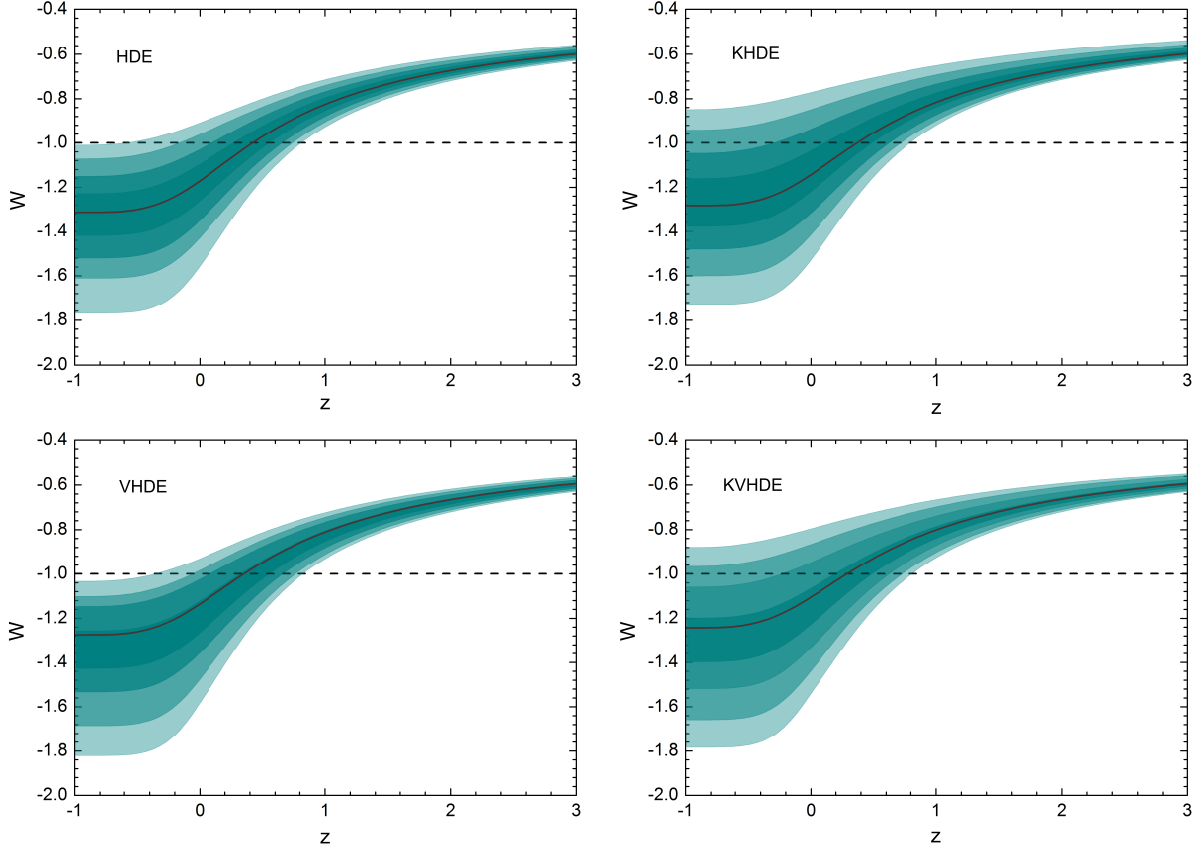


FIG. 7: The evolution of $w(z)$ along with redshift z , including the best-fit results, as well as the $1-4\sigma$ regions, for the considered models.

DR7 and WiggleZ Dark Energy Survey, and the latest measurements of H_0 from HST. In order to treat the perturbations in dark energy when w cross -1 , we employed the PPF method. So, we do not suffer from the divergence problem when w crosses -1 .

We found that, for the simplest HDE model, the phenomenological parameter $c < 1$ at more than 4σ CL, showing that the future Universe will be dominated by phantom dark energy at more than 4σ CL. After taking into account spatial curvature, we have $c < 1$ only in about 2.5σ range, implying that the inclusion of spatial curvature in the holographic dark energy model may be helpful to alleviate the future doomsday problem. In contrast, the inclusion of massive neutrinos does not have significant influence on the phenomenological parameter c .

For the KHDE model, we found that the 2σ range of the spatial curvature is $-0.006 < \Omega_{k0} < 0.020$; moreover, the 3σ error bars of Ω_{k0} are still fairly small, also in order of 10^{-2} . For the VHDE model, we obtained that the 2σ upper bound of the total mass of neutrinos is $\sum m_\nu < 0.48$ eV, which is the first result of neutrino mass in the holographic dark energy model. Moreover, when simultaneously considering

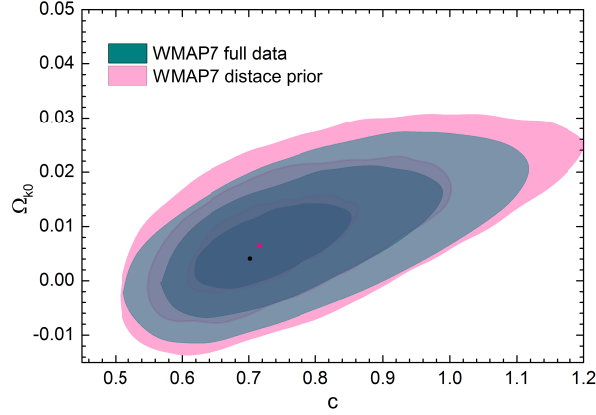


FIG. 8: The marginalized 1, 2, 3 σ CL contours in the c - Ω_{k0} plane, for the KHDE model. The pink contours are plotted by using the WMAP7 distance priors, and the olive contours are plotted by using the full WMAP7 data.

spatial curvature and massive neutrinos, the upper bound of $\sum m_\nu$ will be enlarged by more than 2 times. Furthermore, we also demonstrated that, making use of the full WMAP 7-yr data can give better constraints on the holographic dark energy model, compared with the case using the WMAP “distance priors”.

It should be mentioned that, there are still some factors not covered in our paper, e.g., the interaction between dark sectors. Evidently, when taking into account the interaction, the computation of the dark energy perturbations will become much more complicated. These issues deserve further investigations in the future work.

Acknowledgments

We acknowledge the use of the Legacy Archive for Microwave Background Data Analysis (LAMBDA). Support for LAMBDA is provided by the NASA Office of Space Science. This work was supported by the National Science Foundation of China under Grant Nos. 10705041, 10975032 and 11175042, and by the National Ministry of Education of China under Grant Nos. NCET-09-0276 and N100505001,

-
- [1] A. G. Riess *et al.*, *AJ* **116**, 1009 (1998); S. Perlmutter *et al.*, *ApJ* **517**, 565 (1999).
 - [2] D. N. Spergel *et al.*, *ApJS* **148**, 175 (2003); C. L. Bennet *et al.*, *ApJS* **148**, 1 (2003); D. N. Spergel *et al.*, *ApJS* **170**, 377 (2007); L. Page *et al.*, *ApJS* **170**, 335 (2007); G. Hinshaw *et al.*, *ApJS* **170**, 263 (2007).
 - [3] M. Tegmark *et al.*, *Phys. Rev. D* **69**, 103501 (2004); *ApJ* **606**, 702 (2004); *Phys. Rev. D* **74**, 123507 (2006).
 - [4] V. Sahni and A. Starobinsky, *Int. J. Mod. Phys. D* **9**, 373 (2000); P. J. E. Peebles and B. Ratra, *Rev. Mod. Phys.* **75**, 559 (2003); T. Padmanabhan, *Phys. Rept.* **380**, 235 (2003); E. J. Copeland, M. Sami and S. Tsujikawa, *Int.*

- J. Mod. Phys. D **15**, 1753 (2006); A. Albrecht *et al.*, astro-ph/0609591; J. Frieman, M. Turner and D. Huterer, Ann. Rev. Astron. Astrophys **46**, 385 (2008); S. Tsujikawa, arXiv:1004.1493; V. Sahni and A. Starobinsky, Int. J. Mod. Phys. D **15**, 2105 (2006); M. Li *et al.*, Commun. Theor. Phys. **56**, 525 (2011).
- [5] B. Ratra and P. J. E. Peebles, Phys. Rev. D **37**, 3406 (1988); P. J. E. Peebles and B. Ratra, ApJ **325**, L17 (1988); R. R. Caldwell, R. Dave and P. J. Steinhardt, Phys. Rev. Lett. **80**, 1582 (1998); I. Zlatev, L. Wang and P. J. Steinhardt, Phys. Rev. Lett. **82**, 896 (1999).
- [6] R. R. Caldwell, Phys. Lett. B **545**, 23 (2002); S. M. Carroll, M. Hoffman and M. Trodden, Phys. Rev. D **68**, 023509 (2003); R. R. Caldwell, M. Kamionkowski and N. N. Weinberg, Phys. Rev. Lett. **91**, 071301 (2003).
- [7] C. Armendariz-Picon, T. Damour and V. Mukhanov, Phys. Lett. B **458**, 209 (1999); C. Armendariz-Picon, V. Mukhanov and P. J. Steinhardt, Phys. Rev. D **63**, 103510 (2001); T. Chiba, T. Okabe and M. Yamaguchi, Phys. Rev. D **62**, 023511 (2000).
- [8] T. Padmanabhan, Phys. Rev. D **66**, 021301 (2002); J. S. Bagla, H. K. Jassal, and T. Padmanabhan, Phys. Rev. D **67**, 063504 (2003).
- [9] H. Wei, R. G. Cai, and D. F. Zeng, Class. Quant. Grav. **22**, 3189 (2005); H. Wei, and R. G. Cai, Phys. Rev. D **72**, 123507 (2005); H. Wei, N. N. Tang, and R. G. Cai, Phys. Rev. D **75**, 043009 (2007).
- [10] A. Y. Kamenshchik, U. Moschella and V. Pasquier, Phys. Lett. B **511**, 265 (2001); M. C. Bento, O. Bertolami and A. A. Sen, Phys. Rev. D **66**, 043507 (2002); X. Zhang, F. Q. Wu and J. Zhang, JCAP **0601**, 003 (2006).
- [11] W. Zhao and Y. Zhang, Class. Quant. Grav. **23**, 3405 (2006); T. Y. Xia and Y. Zhang, Phys. Lett. B **656**, 19 (2007); S. Wang, Y. Zhang and T. Y. Xia, JCAP **10** 037 (2008); S. Wang and Y. Zhang, Phys. Lett. B **669** 201 (2008).
- [12] M. Chevallier and D. Polarski, Int. J. Mod. Phys. D **10** 213 (2001); E. V. Linder, Phys. Rev. Lett. **90** 091301 (2003); D. Huterer and G. Starkman, Phys. Rev. Lett. **90** 031301 (2003); D. Huterer and A. Cooray, Phys. Rev. D **71** 023506 (2005); A. Shafieloo, V. Sahni and A. A. Starobinsky, Phys. Rev. D **80** 101301 (2009).
- [13] Q. G. Huang *et al.*, Phys. Rev. D **80** 083515 (2009); S. Wang, X. D. Li and M. Li, Phys. Rev. D **83** 023010 (2011); X. D. Li *et al.*, JCAP **07** (2011) 011; M. Li, X. D. Li and S. Wang, arXiv:0910.0717; S. Wang, X. D. Li and M. Li, Phys. Rev. D **82** 103006 (2010); X. D. Li, S. Wang, Q. G. Huang, X. Zhang and M. Li, Sci. China Phys. Mech. Astron. **55**, 1330 (2012); J. Z. Ma and X. Zhang, Phys. Lett. B **699**, 233 (2011); H. Li and X. Zhang, Phys. Lett. B **703**, 119 (2011); Y. H. Li and X. Zhang, Eur. Phys. J. C **71**, 1700 (2011).
- [14] G. 't Hooft, gr-qc/9310026; L. Susskind, J. Math. Phys. **36**, 6377 (1995).
- [15] A. G. Cohen, D. B. Kaplan and A. E. Nelson, Phys. Rev. Lett. **82**, 4971 (1999).
- [16] M. Li, Phys. Lett. B **603**, 1 (2004).
- [17] M. Li, C. S. Lin and Y. Wang, JCAP **0805**, 023 (2008).
- [18] X. Zhang and F. Q. Wu, Phys. Rev. D **76**, 023502 (2007); Z. Chang, F. Q. Wu and X. Zhang, Phys. Lett. B **633**, 14 (2006); J. Y. Shen, B. Wang, E. Abdalla and R. K. Su, Phys. Lett. B **609**, 200 (2005); Z. L. Yi and T. J. Zhang, Mod. Phys. Lett. A **22**, 41 (2007); M. Li, X. D. Li, S. Wang and X. Zhang, JCAP **0906**, 036 (2009); X. Zhang, Phys. Rev. D **79**, 103509 (2009); Z. P. Huang and Y. L. Wu, arXiv:1202.3517.
- [19] C. J. Hogan, astro-ph/0703775; arXiv:0706.1999; J. W. Lee, J. Lee and H. C. Kim, JCAP **0708**, 005 (2007); M.

- Li *et al.*, Commun. Theor. Phys. **51**, 181 (2009); M. Li and Y. Wang, Phys. Lett. B **687**, 243 (2010); M. Li, R. X. Miao and Y. Pang, Phys. Lett. B **689**, 55 (2010); M. Li, R. X. Miao and Y. Pang, Opt. Express **18**, 9026 (2010).
- [20] Q. G. Huang and Y. G. Gong, JCAP **0408**, 006 (2004); X. Zhang and F. Q. Wu, Phys. Rev. D **72**, 043524 (2005); B. Wang, E. Abdalla and R. K. Su, Phys. Lett. B **611**, 21 (2005); B. Wang, Y. G. Gong and E. Abdalla, Phys. Lett. B **624**, 141 (2005); B. Wang, C. Y. Lin and E. Abdalla, Phys. Lett. B **637**, 357 (2006). S. Nojiri and S. D. Odintsov, Gen. Rel. Grav. **38**, 1285 (2006); J. Zhang, X. Zhang and H. Y. Liu, Eur. Phys. J. C **52**, 693 (2007); C. J. Feng, Phys. Lett. B **633**, 367 (2008); H. Wei and R. G. Cai, Phys. Lett. B **655**, 1 (2007); R. G. Cai, Phys. Lett. B **657**, 228 (2007); C. Gao, F. Wu, X. Chen and Y. G. Shen, Phys. Rev. D **79**, 043511 (2009); Y. Z. Ma, Y. Gong and X. L. Chen, Eur. Phys. J. C **60**, 303 (2009). C. J. Feng and X. Zhang, Phys. Lett. B **680**, 399 (2009); J. F. Zhang *et al.*, Eur. Phys. J. C **72**, 2077 (2012).
- [21] Q. G. Huang and M. Li, JCAP **0408**, 013 (2004).
- [22] Q. G. Huang and M. Li, JCAP **0503**, 001 (2005); X. Zhang, Int. J. Mod. Phys. D **14**, 1597 (2005); Phys. Lett. B **648**, 1 (2007); Phys. Rev. D **74**, 103505 (2006); B. Chen, M. Li and Y. Wang, Nucl. Phys. B **774**, 256 (2007); J. F. Zhang, X. Zhang and H. Y. Liu, Phys. Lett. B **651**, 84 (2007); H. Wei and S. N. Zhang, Phys. Rev. D **76**, 063003 (2007); M. R. Setare, J. F. Zhang and X. Zhang, JCAP **0703**, 007 (2007); J. F. Zhang, X. Zhang and H. Y. Liu, Phys. Lett. B **659**, 26 (2008); Y. Z. Ma and X. Zhang, Phys. Lett. B **661**, 239 (2008); B. Nayak and L. P. Singh, Mod. Phys. Lett. A **24**, 1785 (2009); K. Y. Kim, H. W. Lee and Y. S. Myung, Mod. Phys. Lett. A **24**, 1267 (2009); Y. G. Gong and T. J. Li, Phys. Lett. B **683**, 241 (2010); Z. P. Huang and Y. L. Wu, arXiv:1202.4228.
- [23] X. Zhang, Phys. Lett. B **683**, 81 (2010).
- [24] H. C. Kao, W. L. Lee, F. L. Lin, Phys. Rev. D **71**, 123518 (2005).
- [25] Y. Gong, B. Wang, Y. Z. Zhang, Phys. Rev. D **72**, 043510 (2005).
- [26] M. Li, X. Li and X. Zhang, Sci. China Phys. Mech. Astron. **53**, 1631 (2010).
- [27] Z. Zhang *et al.*, Mod. Phys. Lett. A, **27**, 1250115 (2012).
- [28] Z. Zhang *et al.*, JCAP **06**, 009 (2012).
- [29] L. Xu, Phys. Rev. D **85**, 123505 (2012).
- [30] R. Amanullah *et al.*, Astrophys. J. **716**, 712 (2010).
- [31] W. J. Percival *et al.*, MNRAS **401**, 2148 (2010).
- [32] E. Komatsu *et al.*, ApJS. **192**, 18 (2011).
- [33] C. Clarkson, M. Cortes and B. A. Bassett, JCAP **0708**, 011 (2007).
- [34] H. Li and X. Zhang, Phys. Lett. B **713**, 160 (2012).
- [35] W. Fang, *et al.*, Phys. Rev. D **78** 103509 (2008); W. Fang, W. Hu, and A. Lewis, Phys. Rev. D **78** 087303 (2008).
- [36] E. Komatsu *et al.*, ApJS. **180**, 330 (2009).
- [37] A. Lewis and S. Bridle, Phys. Rev. D **66**, 103511 (2002).
- [38] D. Spergel, *et al.*, Astrophys. J. Suppl. **170** 377 (2007).
- [39] J. Weller and A. Lewis, Mon. Not. R. Astron. Soc. **346** 987 (2003).
- [40] J. Q. Xia, G. B. Zhao, B. Feng, H. Li, X. M. Zhang, Phys. Rev. D **73** 063521 (2006).
- [41] C. P. Ma and E. Bertschinger, Astrophys. J. **455** 7 (1995).

- [42] G. B. Zhao, J. Q. Xia, M. Li, B. Feng and X. M. Zhang, Phys. Rev. D **72**, 123515 (2005).
- [43] W. Hu and I. Sawicki, Phys. Rev. D **76** 104043 (2007); W. Hu, Phys. Rev. D **77** 103524 (2008).
- [44] A. G. Sanchez, *et al.*, arXiv:1203.6616, MNRAS accepted.
- [45] <http://lambda.gsfc.nasa.gov/>.
- [46] N. Suzuki *et al.*, arXiv:1105.3470.
- [47] M. Drinkwater *et al.*, MNRAS **401**, 1429 (2010); C. Blake *et al.*, arXiv:1108.2635, MNRAS accepted.
- [48] A. G. Riess *et al.*, Astrophys. J. **730**, 119 (2011).
- [49] M. Li *et al.*, JCAP **12**, 014 (2009).